Diabetology & Metabolic Syndrome

RESEARCH

Open Access

Strategy for treating MAFLD: Electroacupuncture alleviates hepatic steatosis and fibrosis by enhancing AMPK mediated glycolipid metabolism and autophagy in T2DM rats

Haoru Duan[1,2†], Shanshan Song[1,3†], Rui Li[1*], Suqin Hu[4], Shuting Zhuang[1], Shaoyang liu[1], Xiaolu Li[1] and Wei Gao[1]

Abstract

Background Recent studies have highlighted type 2 diabetes (T2DM) as a significant risk factor for the development of metabolic dysfunction-associated fatty liver disease (MAFLD). This investigation aimed to assess electroacupuncture's (EA) impact on liver morphology and function in T2DM rats, furnishing experimental substantiation for its potential to stall MAFLD progression in T2DM.

Methods T2DM rats were induced by a high-fat diet and a single intraperitoneal injection of streptozotocin, and then randomly assigned to five groups: the T2DM group, the electroacupuncture group, the metformin group, combination group of electroacupuncture and metformin, combination group of electroacupuncture and Compound C. The control group received a standard diet alongside intraperitoneal citric acid - sodium citrate solution injections. After a 6-week intervention, the effects of each group on fasting blood glucose, lipids, liver function, morphology, lipid droplet infiltration, and fibrosis were evaluated. Techniques including Western blotting, qPCR, immunohistochemistry, and immunofluorescence were employed to gauge the expression of key molecules in AMPK-associated glycolipid metabolism, insulin signaling, autophagy, and fibrosis pathways. Additionally, transmission electron microscopy facilitated the observation of liver autophagy, lipid droplets, and fibrosis.

Results Our studies indicated that hyperglycemia, hyperlipidemia and IR promoted lipid accumulation, pathological and functional damage, and resulting in hepatic steatosis and fibrosis. Meanwhile, EA enhanced the activation of AMPK, which in turn improved glycolipid metabolism and autophagy through promoting the expression of PPARα/CPT1A and AMPK/mTOR pathway, inhibiting the expression of SREBP1c, PGC-1α/PCK2 and TGFβ1/Smad2/3 signaling pathway, ultimately exerting its effect on ameliorating hepatic steatosis and fibrosis in T2DM rats. The above effects of

†Haoru Duan and Shanshan Song contributed equally to this work and shared first authorship.

*Correspondence:
Rui Li
tingxuezhai@126.com

Full list of author information is available at the end of the article

EA were consistent with metformin. The combination of EA and metformin had significant advantages in increasing hepatic AMPK expression, improving liver morphology, lipid droplet infiltration, fibrosis, and reducing serum ALT levels. In addition, the ameliorating effects of EA on the progression of MAFLD in T2DM rats were partly disrupted by Compound C, an inhibitor of AMPK.

Conclusions EA upregulated hepatic AMPK expression, curtailing gluconeogenesis and lipogenesis while boosting fatty acid oxidation and autophagy levels. Consequently, it mitigated blood glucose, lipids, and insulin resistance in T2DM rats, thus impeding liver steatosis and fibrosis progression and retarding MAFLD advancement.

Keywords Type 2 diabetes, Metabolic dysfunction-associated fatty liver disease, Electroacupuncture, AMP-activated protein kinase signaling pathway, Autophagy

Introduction

Non-Alcoholic Fatty Liver Disease (NAFLD), recently redefined as Metabolic Associated Fatty Liver Disease (MAFLD), presents a significant health burden worldwide, particularly among individuals with Type 2 Diabetes Mellitus (T2DM). The progression of MAFLD from simple hepatic steatosis to steatohepatitis and fibrosis poses substantial risks to affected individuals, particularly those with comorbid T2DM [1]. Studies had consistently shown that T2DM patients faced a substantially elevated risk up to 70 −80% of developing MAFLD compared to non-diabetic counterparts [2–4]. Importantly, the convergence of T2DM and MAFLD escalated the risk of cardiovascular complications due to compromised metabolic control [5–8]. A recent prospective case-control study involving 2103 T2DM patients underscored this risk, revealing an association between MAFLD and increased cardiovascular disease risk over a five-year follow-up period, even after adjustments for other pertinent risk factors were made [9]. Hence, the evaluation and management of MAFLD, even in its milder forms, are imperative for mitigating cardiovascular risk and improving overall mortality rates among individuals with T2DM.

The pathological process of MAFLD is intricately intertwined with insulin resistance (IR), a condition characterized by decreased sensitivity of cells to the effects of insulin hormone. In MAFLD initiation, the primary manifestation is simple steatosis, characterized by the accumulation of triglycerides (TG) in over 5% of hepatocytes [10, 11]. This accumulation is significantly influenced by IR, which serves as a driving force in the development and progression of MAFLD. One of the key consequences of IR is the increased influx of fatty acids into the liver, which, coupled with elevated hepatic de novo lipogenesis (DNL), results in heightened TG levels within hepatocytes [12–14]. Furthermore, inhibition of peroxisome proliferator-activated receptor alpha (PPARα) and carnitine palmitoyltransferase 1 (CPT1) reduces fatty acid oxidation (FAO), further contributing to TG accumulation [10, 15]. The failure of insulin to effectively regulate liver glucose uptake and production exacerbates hyperglycemia and IR, thereby exacerbating the pathogenic processes underlying MAFLD [16]. Persistent IR, coupled with increased free fatty acid (FFA) influx, induces mitochondrial dysfunction, reactive oxygen species (ROS) production, and toxic lipid accumulation, which in turn exacerbates hepatic damage [17]. As MAFLD progresses, it encompasses fatty infiltration, lobular inflammation, and can manifest into severe forms such as non-alcoholic steatohepatitis (NASH) [18, 19]. NASH, if left unchecked, may advance to perisinusoidal fibrosis, cirrhosis, and ultimately hepatocellular carcinoma (HCC) [1, 20, 21]. Given the reversible nature of MAFLD in its early stages, timely intervention becomes paramount in altering its trajectory and curbing its escalating prevalence [22, 23]. Thus, there is an imperative need to address the underlying pathological factors, particularly focusing on interventions aimed at mitigating diabetes-induced liver injury.

Autophagy, a cellular process essential for maintaining homeostasis, serves as a protective mechanism against liver injury induced by various metabolic insults [24–26]. Specifically, in the context of MAFLD, dysregulated lipid metabolism and oxidative stress overwhelms cellular defenses, leading to hepatocyte dysfunction and the progression of liver pathology. Autophagy in hepatocytes plays a pivotal role in mitigating these effects by removing damaged organelles and lipid droplets, thus preventing excessive cell death and fibrosis [24, 27]. However, when autophagy is impaired, as seen in MAFLD, the liver becomes more susceptible to injury and fibrotic progression [28–30]. Studies have demonstrated that knocking out autophagy-related genes exacerbates hepatic fibrosis, underscoring the protective role of autophagy in liver pathology [31].

To optimize therapeutic outcomes in MAFLD, addressing metabolic disturbance, steatosis, and liver damage is crucial [32]. One promising strategy for the treatment of T2DM-induced MAFLD involves targeting the AMP-activated protein kinase (AMPK) pathway, which plays a crucial role in cellular energy homeostasis and metabolism regulation [33]. Activation of AMPK has been shown to enhance glycolipid metabolism and autophagy,

both of which are essential processes for mitigating the adverse effects of insulin resistance in MAFLD. By enhancing glycolipid metabolism, AMPK activation alleviates the excess accumulation of triglycerides in hepatocytes by promoting the conversion of glucose into energy rather than storing it as lipids [34–37]. Additionally, autophagy induction facilitated by AMPK activation can aid in the removal of damaged mitochondria and toxic lipid species, thus mitigating the progression of hepatic damage in MAFLD [38, 39]. Moreover, targeting AMPK signaling also improves insulin sensitivity, thereby addressing one of the central pathological features of MAFLD [40]. Therefore, interventions aimed at enhancing AMPK-mediated glycolipid metabolism and autophagy hold promise as potential therapeutic avenues for addressing insulin resistance in the pathological process of MAFLD. While several compounds are undergoing clinical investigation for MAFLD management, none have received specific approval yet [41]. Acupuncture, a unique external therapy in traditional Chinese medicine with a lengthy history of treating T2DM in China, has been reported to be effective against T2DM, IR, and diabetic liver injury [42–45]. Recent studies, including our unpublished research, had indicated that EA's hypoglycemic and hypolipidemic effects protected the liver's morphology and function in T2DM rats by reducing inflammation and lipid droplet infiltration in liver tissue [46, 47]. These findings underscored EA's therapeutic potential in ameliorating T2DM with MAFLD, with the underlying molecular mechanism associated with AMPK activation. Building upon these promising results and "prevent before the disease exacerbats" thought in traditional chinese medicine (TCM), we hypothesized that EA might prevent hepatic steatosis and fibrosis in diabetes-induced hepatic dysfunction by enhancing the AMPK signaling pathway, resulting in the upregulation of glycolipid metabolism and autophagy and inhibiton of TGFβ/SMAD3 signaling pathways. Therefore, our present study primarily investigated EA's potential effect and mechanism of treatment and its specific relationship with hepatoprotection and anti-fibrosis in T2DM rats induced by a high-fat diet (HFD) and injection of STZ, aiming to provide therapeutic strategies for preventing or delaying the progression of MAFLD.

Materials and methods

Establishment of T2DM animal model

Male Wistar rats of Specific Pathogen Free (SPF) grade, weighing 150–180 g, were procured from Sibeifu (Beijing) Biotechnology Co., Ltd. These rats were maintained at 23 ± 2 °C, with a humidity of 40% ± 5%, under a 12-hour light/dark cycle. After acclimatization for 7 days, 10 rats were randomly assigned to the Control group (Con), provided with ad libitum access to water and standard rat chow. The remaining rats were induced to develop a T2DM model through a high-fat diet combined with streptozotocin (STZ) injection. The induction protocol involved feeding the rats a high-fat diet (comprising 67% regular rodent chow, 20% sucrose, 10% lard, 2.5% cholesterol, and 0.5% sodium cholate) for 4 weeks, followed by an overnight fast of 20 h, and subsequent intraperitoneal injection with a 2% solution of streptozocin (STZ) (dissolved in 0.1 mmol/L citrate buffer solution with a pH of 4.2–4.5) at a dose of 35 mg/kg. The Con group rats were intraperitoneally injected with 0.1 mol/L pH=4.2 citric acid - sodium citrate buffer. The criterion for successful T2DM model preparation was set as Random Blood Glucose (RBG) ≥ 16.7mmol/L and/or Fasting Blood Glucose (FBG) ≥ 11.1 mmol/L [48, 49]. Throughout the 14-day model evaluation and 6-week interventions, rats, excluding those in the Con group, were fed a high-fat diet. A total of 60 rats were included as model animals, and they were randomly allocated into the following groups based on FBG levels: Control (Con), T2DM, Electroacupuncture (EA), Metformin (Met), Electroacupuncture combined with Metformin (EA+Met), and Electroacupuncture combined with Compound C (EA+Compd C), each comprising 10 rats.

Rats with EA treatment involved the use of disposable sterile acupuncture needles (0.13*7 mm) at bilateral acupoints, including Pishu (BL 19), Weiwanxiashu (EX B3), Zusanli (ST 36), and Sanyinjiao (SP 6). The needles were inserted to a depth of 4–6 mm. Additionally, Weiwanxiashu (EX B3) and Zusanli (ST 36) were connected to an electroacupuncture instrument set to a continuous wave, with a frequency of 15 Hz and an amplitude of 2–4 mA, for 20 min per session, Once a day. In contrast, rats in the Met group received a daily gavage of 60 mg/mL metformin solution, dosed at 5 mL/kg body weight. Meanwhile, rats in the EA+Met group underwent both EA and Met treatment once a day. The EA session lasted for 20 min, while a 60 mg/mL metformin solution was administered at a dosage of 5 mL/kg. Another group, the EA+Compd C group, was subjected to intraperitoneal injection of Compound C at a dosage of 10 mg/kg, in addition to the daily 20-minute acupuncture session. Rats in the control and T2DM groups underwent immobilization similar to that of the EA group but without any other interventions. All interventions were carried out six times a week over the six-week period. At the end of the six-week intervention, the rats were sacrificed for further analysis. Plasma and liver samples were collected and stored for subsequent examinations.

Measurement of FBG, blood lipids, weight, serum insulin (INS), aspartate aminotransferase (AST), alanine aminotransferase (ALT) and albumin (ALB)

FBG levels of all rats were measured through tail vein using the Roche Accu-Chek blood glucose meter before modeling, before intervention, and at the end of each week during the intervention period, following a 12-hour fast. The animal weight were measured before modeling, before and after intervention. The serum was separated through centrifugation at 3000 r/min, at 4℃ for 15 min, and serum concentrations of TC, TG, LDL, HDL, AST, ALT and ALB were determined by enzyme colorimetry. Insulin levels were measured by radioimmunoassay. Homeostasis model assessment of insulin resistance (HOMA-IR) and insulin sensitivity (HOMA-ISI) were computed with the following formula: HOMA-IR = (Fasting glucose (mmol/L) × Fasting serum insulin (μU/mL))/22.5. HOMA-ISI=22.5 / {Fasting glucose (mmol/L) × fasting serum insulin (μU/mL)}.

Hematoxylin-eosin (HE) staining

Hematoxylin and eosin (H&E) staining was performed to examine liver morphology. Livers were collected in 4% paraformaldehyde solution for 24 h, and embedded in paraffin wax blocks after dehydrating through a serial alcohol gradient. All sections were cut at 5 μm sections through a microtome, and processed for staining with H&E. After staining, the sections were dehydrated with ascending concentrations of ethanol and xylene. Images were captured using an optical microscope (BX53; Olympus Optical).

Oil red O staining (G1261)

Oil Red O staining was used to evaluate liver steatosis. Mix Oil Red O stain A and B with the radio of 3:2 and place for 10 min to form modified Oil Red O stain solution. 10-μm-thick frozen liver sections were washed by water after fix in 10% formalin for 10 min and soaked in 60% isopropanol for 30s. Staining was performed in modified Oil Red O stain solution for 10 min. The tissue slices were placed in 60% isopropanol to continue colour separation. After staining, the sections were staining by Mayer's Hematoxylin solution for 1 min and rinsed by tap water for 10 min. Images were captured using an optical microscope (BX53; Olympus Optical).

Masson staining (G1346)

Masson staining was used to evaluate liver fibrosis. 5-μm-thick paraffin sections were routinely dewaxed to distilled water and incubated in Mordant Solution (12 h), Celestite Blue Solution (2 min), Mayer hematoxylin (2 min). After differentiation with Acid Differentiation Solution, the sections were washed with distilled water to stop differentiation, and then treated with Ponceau-Acid Fuchsin Solution (10 min), Phosphomolybdic Acid Solution (10 min), Aniline Blue Solution (5 min). Images were captured using an optical microscope (BX53; Olympus Optical).

Immunohistochemical staining

The liver paraffin sections underwent dewaxing to water and were subsequently subjected to heating in sodium citrate antigen retrieval solution in a microwave oven for 15 min. Following PBS washing, goat serum was applied to block the sections for 10 min. A specific primary antibody (listed in Supplementary Table 1) was then applied for overnight incubation at 4 ℃, succeeded by incubation with immunohistochemical secondary antibodies for 10 min at room temperature. After a 3-minute incubation with DAB solution, all sections were examined using an optical microscope (Nikon 80i, Japan).

Immunofluorescence staining

The liver paraffin sections were dewaxed to water and heated in sodium citrate antigen retrieval solution in a microwave oven for 15 min. Subsequent to PBS washing, the sections were blocked with immunostaining blocking solution for 1 h. Overnight incubation with a specific primary antibody (listed in Supplementary Table 1) at 4 ℃ was followed by incubation with fluorescent secondary antibodies for 2 h at room temperature in the dark. After a 5-minute incubation with DAPI, all sections were observed via fluorescent microscopy (Nikon 80i, Japan).

Western blotting

Liver tissue was lysed using RIPA lysis buffer containing protein phosphatase inhibitor, followed by centrifugation at 12,000×g, 4℃ for 10 min, and the supernatant was collected. Same amount of protein sample was separated by SDS–polyacrylamide gel electrophoresis and transferred onto PVDF membranes. The membranes were blocked with 5% skim milk solution for 2 h, then incubated with primary antibodies (listed in Supplementary Table 2) at 4℃ overnight. After thrice washing for 10 min with TBST, the membranes were incubated with HRP-conjugated Affinipure Goat Anti-Mouse IgG (1:10000) or HRP-conjugated Affinipure Goat Anti-Rabbit IgG (=1:20000) for 1.5 h at room temperature. The target proteins were visualized using an enhanced chemiluminescence substrate and chemiluminescence imaging system. Band intensities were detected and analyzed using image J software, Version 1.8.0.112 (National Institutes of Health (NIH)).

Quantitative PCR (qPCR)

The extraction of total RNA utilized the HiPure Total RNA Mini Kit, followed by reverse transcription using the Reveaid First Strand cDNA Synthesis Kit. For qPCR

analysis, 2 μl of the resulting cDNA underwent amplification and measurement employing the Power Sybr Green PCR Master Mix. Reactions were executed on a Bio-Rad CFX Maestro 1.0 ABI PRISM 7300 real-time cycler (Applied Biosystems, Foster City, CA). The protocol included a melting step at 95 °C for 10 min, followed by 49 amplification cycles (95 °C, 10 s; 55 °C, 30 s; 65 °C, 5 s). mRNA levels for each gene were determined utilizing the ΔΔCT method with GAPDH serving as a reference. The primers utilized for RT-PCR are detailed in Table 3.

Transmission electron microscope

Liver tissue specimens were meticulously processed to ensure accurate characterization of microstructural alterations underlying metabolic associated fatty liver disease (MAFLD) pathogenesis. Initially, liver samples were meticulously fixed in 2.5% glutaraldehyde solution. Subsequently, a systematic dehydration process was employed utilizing a graded series of ethanol concentrations ranging from 30 to 100%, facilitating the removal of water from the tissue while maintaining structural integrity. Following dehydration, the specimens underwent critical point drying to further eliminate residual moisture. To enhance electron conductivity and imaging quality, the dehydrated liver samples were coated with a thin layer of platinum via sputtering. Ultrastructural observations of liver microarchitecture were performed utilizing a transmission electron microscope (JEM-1400, Japan).

Statistical analysis

Quantitative data were presented as mean values accompanied by standard error of mean (SEM). Statistical comparisons were conducted employing rigorous analytical methods, including one-way analysis of variance (ANOVA) followed by the Student-Newman-Keuls post-hoc test to determine intergroup differences. Significance levels were set at $P<0.05$, ensuring robust statistical evaluation and interpretation of experimental findings.

Results

Influence of EA on glycolipid metabolism and insulin resistance in T2DM model rats

Figure 1A, B depicted significant weight and FBG level increases in T2DM rats before intervention, confirming successful T2DM model establishment. Throughout the study, FBG levels in the T2DM group continued to rise, significantly peaking post-intervention. Compared to pre-intervention levels, FBG concentrations in EA, Met, and EA+Met groups notably decreased after the fourth, fifth, and sixth weeks of treatment. However, the FBG levels in the EA+Met group, although the lowest, did not show statistical significance compared to the other groups. Conversely, FBG levels in the EA+Compd C group were markedly higher than those in the EA group post-intervention. FBG levels in the Con group remained within the normal range throughout the study. Following intervention, T2DM rats exhibited insulin resistance and lipid metabolism disturbances. Serum TC, TG, LDL, weight, and HOMA-IR levels significantly surpassed those of the Con group, while serum HDL levels and HOMA-ISI notably decreased in the T2DM group. Conversely, all treatment groups showed significant reductions in TC, TG, LDL, weight, and HOMA-IR levels, with notable increases in HDL levels and HOMA-ISI (Fig. 1B-D).

EA ameliorated hepatic function and morphological change in T2DM rats

As shown in Fig. 2A, histopathological analysis (H&E staining) revealed evident liver damage in T2DM rats, characterized by hepatocyte swelling, lipid vacuoles, ballooning, inflammation, and lobular structure irregularities. Notably, after 6 weeks of EA and Met treatment, these pathological features improved significantly, with EA+Met nearly restoring hepatocyte morphology to normal levels, indicating a potent synergistic effect of the two interventions. Furthermore, staining with Oil Red O (Fig. 2B), a dye commonly used to visualize lipid droplets, demonstrated substantial lipid accumulation in T2DM rat livers compared to the Con group, which decreased significantly after EA and Met treatment, suggesting an attenuation of hepatic steatosis—a prevalent complication in T2DM-associated liver dysfunction. The combined group exhibited lower lipid accumulation than the EA or Met groups. Masson staining was used to detect collagenous fibers and evaluate hepatic fibrosis. In Fig. 2C, the Masson staining revealed a stark contrast between the normal and model groups in terms of hepatic fibrosis, with the model group displaying a significant increase in collagen fibers, which was significantly improved in the EA group and Met group (Fig. 2C). It is worth noting that the degree of liver fibrosis infiltration in the EA+Met group was significantly better than that in the EA group and metformin group, approaching the Con group, indicating the advantages of EA+Met intervention in improving T2DM-induced hepatic fibrosis. Furthermore, serum AST, ALT, and ALB levels, the critical hepatic function indicators, were used to appraise the hepatoprotective effect of EA, Met and EA+Met in T2DM rats (Fig. 2D). In rats with T2DM, serum AST and ALT levels exhibited a decline, concomitant with an elevation in serum ALB levels. Upon administering three distinct treatments (EA, Met, EA+Met), the trend in AST and ALT levels showed a obvious decrease, whereas ALB levels experienced a subsequent increase. Remarkably, the combined approach of EA alongside medication demonstrated superior efficacy in modulating ALT levels compared to both metformin monotherapy and EA

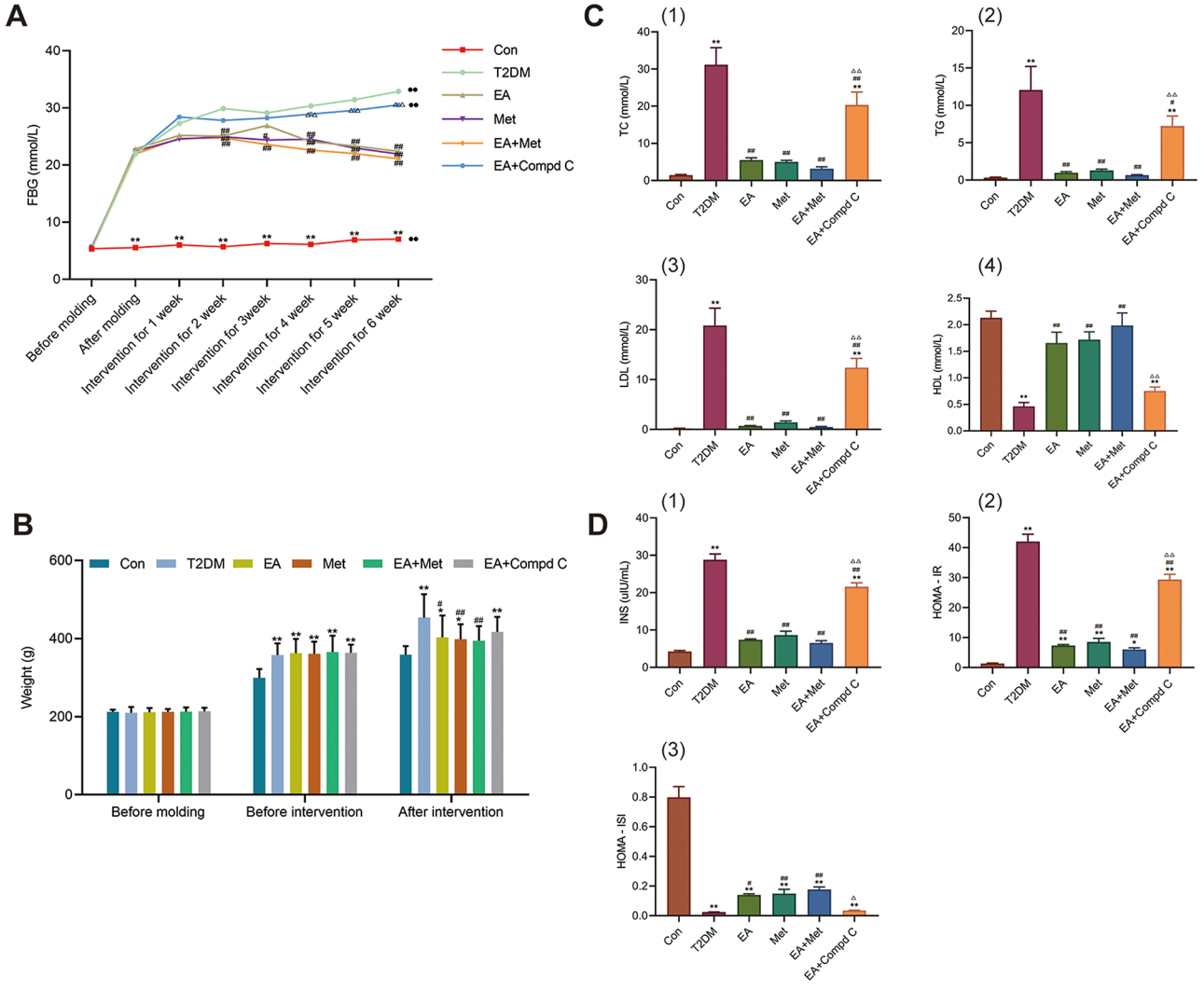

Fig. 1 The effects of EA on the levels of FBG, serum lipid, and insulin in T2DM model rats. **A**: Fasting blood glucose, **B**:Weight, **C**: [1] TC, [2] TG, [3] LDL, [4] HDL, **D**: [1] insulin (INS), [2] insulin resistance index (HOMA-IR) and [3] insulin sensitivity index (HOMA-ISI). Con: the control group, T2DM: the T2DM group, EA: the electroacupuncture group, Met: the metformin group, EA + Met: combination group of electroacupuncture and metformin, EA + Compd C: combination group of electroacupuncture and compound C. Data are expressed as mean ± standard error of mean ($n = 10$ rat per group). Compared with the Con group, $^{*}P < 0.05$, $^{**}P < 0.01$; compared with the T2DM group, $^{\#}P < 0.05$, $^{\#\#}P < 0.01$; compared with the EA group, $P < 0.05$, $P < 0.01$; compared with the same group before intervention, $P < 0.05$, $P < 0.01$

interventions, as shown in Fig. 2D [2]. This finding not only underscored the potential synergistic effects of combining therapeutic modalities but also highlighted EA's promising role in ameliorating hepatic function in the context of T2DM.

EA improved the expression of glycolipid metabolism and insulin signaling pathways mediated by AMPK in T2DM rats

AMPK, a key regulator of fatty acid, glucose homeostasis, and insulin sensitivity, was investigated along with its downstream signaling pathways PPARα/CPT1A, SREBP1c and PGC-1α/PCK2, which responsible for gluconeogenesis, fat generation, and fatty acids oxidative utilization. In the results shown in Figs. 1 and 2, we observed an interesting phenomenon. In the EA + Compd C group, the effects of EA on lowering fasting blood glucose and lipids, alleviating insulin resistance, and improving the liver morphology and function in T2DM rats were partially reversed by Compound C, a specific inhibitor of AMPK. Therefore, we detected the expression of AMPK in the liver of rats in each group using Western Blotting, qPCR, and immunohistochemical staining methods (Fig. 3A- 1 and A-2 and A-3), to explore the relationship between the therapeutic effect of EA and AMPK expression. The results of all three detection methods showed that the AMPK expression in the liver of T2DM group was lower than that of the Con group.

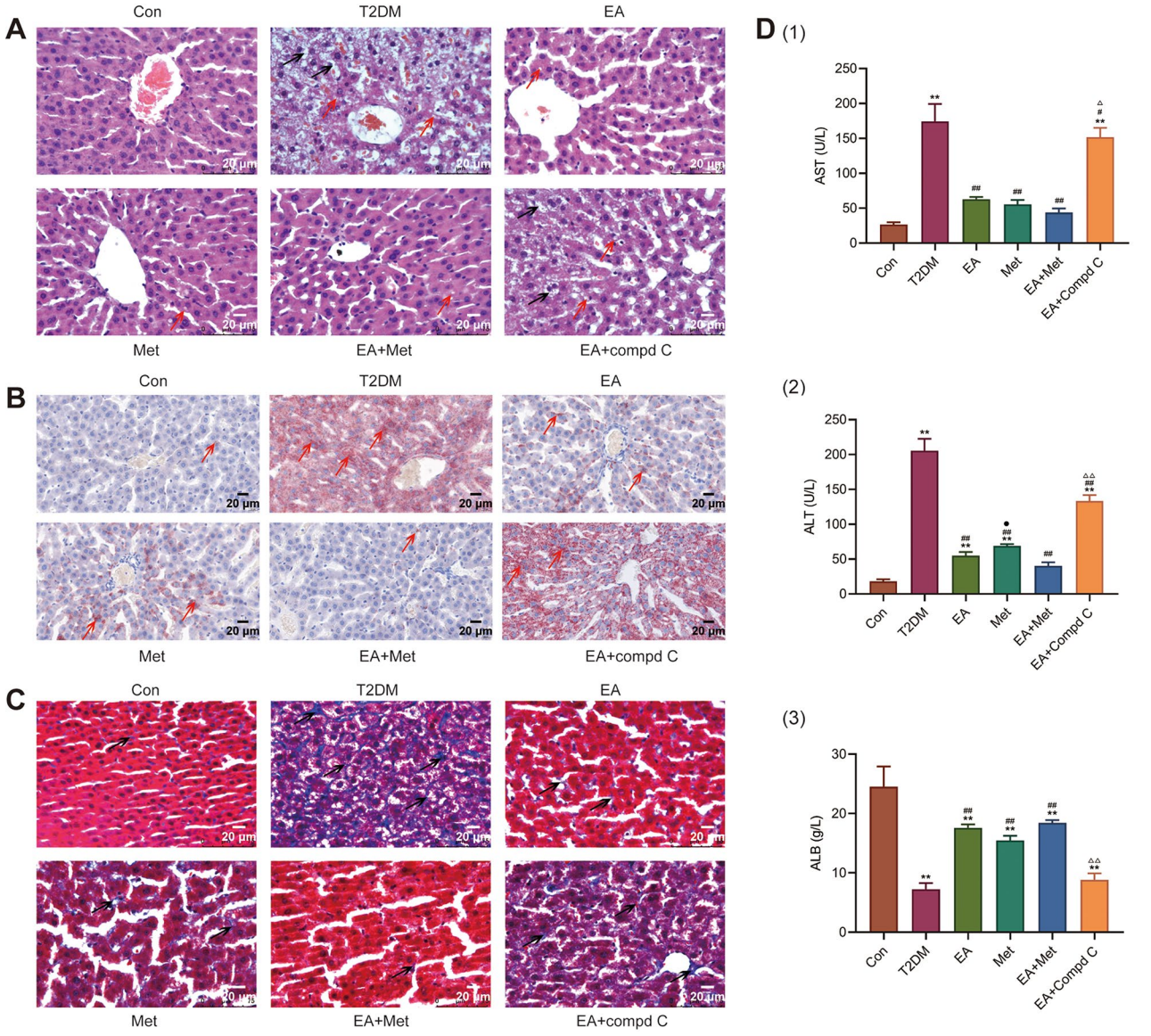

Fig. 2 The effects of EA on the morphology and function of the liver in T2DM model rats. **A**: HE staining showed hepatic histological changes after intervention (red arrow: hepatocytic lipid vacuoles, black arrow: hepatocyte ballooning). Images are shown at the original magnification of 400×. **B**: Oil Red O staining evaluated liver steatosis (red arrow: lipid droplets). Images are shown at the original magnification of 400×. **C**: Masson staining evaluated liver fibrosis (black arrow: collagen fibers). Images are shown at the original magnification of 400×. **D**: levels of serum [1] AST, [2] ALT, [3] ALB ($n=10$ per group). Con: the control group, T2DM: the T2DM group, EA: the electroacupuncture group, Met: the metformin group, EA + Met: combination group of electroacupuncture and metformin, EA + Compd C: combination group of electroacupuncture and compound C. Data are expressed as mean ± standard error of mean. Compared with the Con group, $^{**}P<0.01$; compared with the T2DM group, $^{\#}P<0.05$, $^{\#\#}P<0.01$; compared with the EA group, $^{\triangle}P<0.05$, $^{\triangle\triangle}P<0.01$; compared with the EA + Met group, $^{\bullet}P<0.05$

Contrary to the T2DM group, EA significantly increased the expression of AMPK in the liver. However, the effect of EA on upregulating AMPK expression was reversed with the action of AMPK inhibitor, which indicated that AMPK is one of the important targets of EA. The results of the above three detection methods also showed that Met and EA + Met also had the same effect as EA, that is, to reverse the reduction in hepatic AMPK expression in the T2DM rats. It is worth noting that in immunohistochemical staining, the expression of hepatic AMPK in the EA + Met group was significantly higher than that in the EA group and Met group, partially indicating the synergistic effect of acupuncture drug combination on AMPK expression (Fig. 3A-3).

We also detected the molecular expression on the downstream metabolic pathway of AMPK, and the results indicated that PPARα and CPT1A protein expression were distinctly suppressed, while PGC-1α and PCK2 protein expression were distinctly upgraded by HFD + STZ treatment as compared to the Con group.

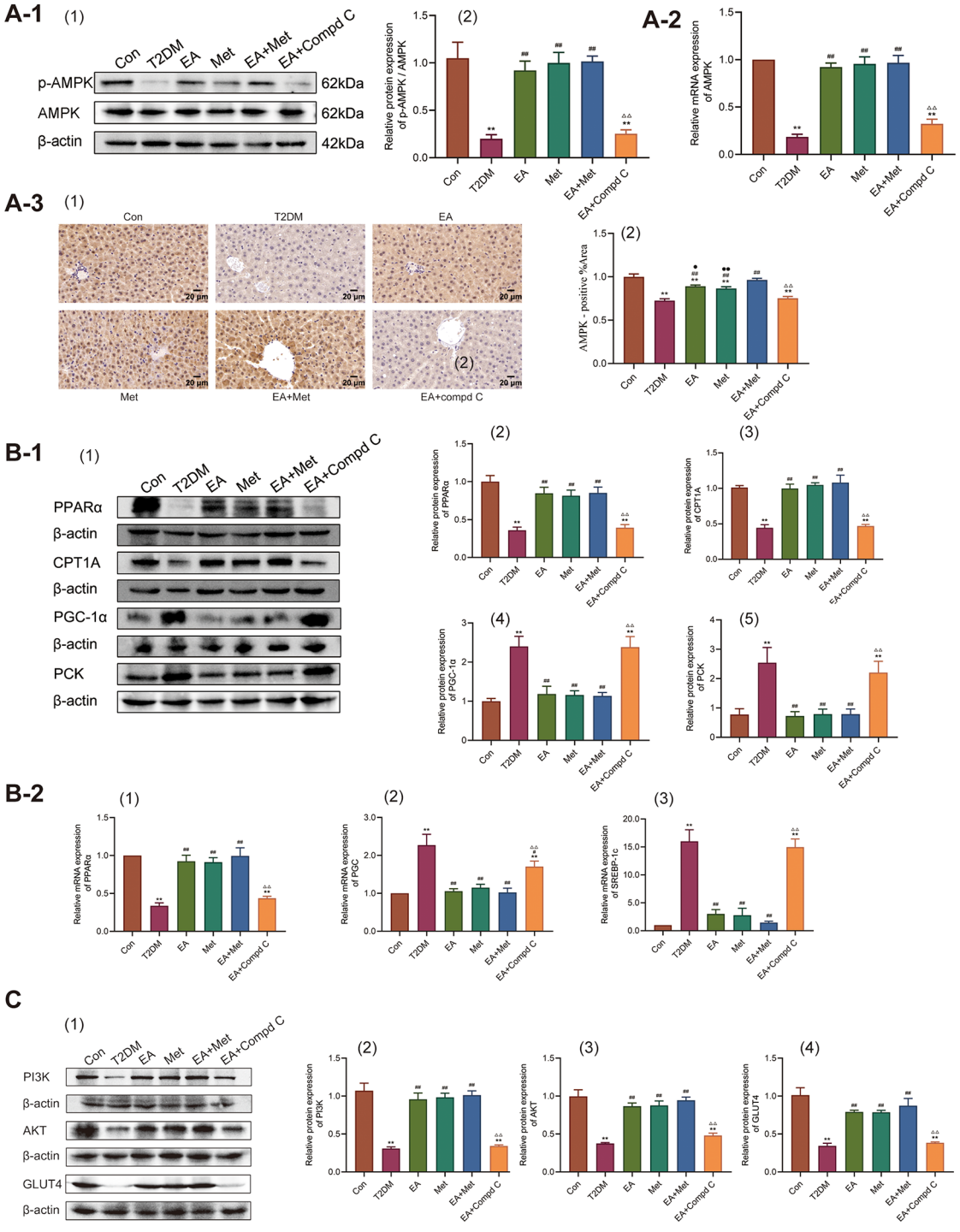

Fig. 3 The effects of EA on the expression of glycolipid metabolism and insulin signaling pathways mediated by AMPK in T2DM model rats. **A**-1: [1] Protein expression of hepatic AMPK. [2] Quantification of protein levels of p-AMPK/AMPK ($n=3$ per group). **A**-2: mRNA levels of AMPK ($n=6$ per group). **A**-3: [1] Representative images of immunohistochemical staining of AMPK expressions in the liver. Images are shown at the original magnification of 400×. [2] Quantitative analyses according to groups ($n=6$ per group). **B**-1: [1] Protein expression of hepatic glycolipid metabolism signaling pathways. [2-5] Quantification of protein levels of PPARα, CPT1A, PGC1-α, PCK2 ($n=3$ per group). **B**-2: [1-3] mRNA levels of PPARα, SREBP1c, PGC1-α ($n=6$ per group). **C**: [1] Protein expression of hepatic insulin signaling transduction pathway. [2-4] Quantification of protein levels of PI3K, AKT, GLUT4 ($n=3$ per group). Con: the control group, T2DM: the T2DM group, EA: the electroacupuncture group, Met: the metformin group, EA + Met: combination group of electroacupuncture and metformin, EA + Compd C: combination group of electroacupuncture and compound C. Data are expressed as mean ± standard error of mean. Compared with the Con group, $^{**}P<0.01$; compared with the T2DM group, $^{\#\#}P<0.01$; compared with the EA group, $P<0.01$; compared with the EA + Met group, $P<0.05$, $P<0.05$

However, EA, Met and EA+Met treatment reversed the changes of PPARα, CPT1A, PGC-1α and PCK2 protein expression in T2DM rats (Fig. 3B-1). The results of qPCR further confirmed that the mRNA levels of PGC-1α and SREBP-1c were significantly increased in T2DM group and decreased by EA, Met and EA+Met treatment, meanwhile the mRNA levels of PPARα were decreased in T2DM group and increased in EA, Met and EA+Met groups (Fig. 3B-2). The phosphoinositide 3-kinase (PI3K) / protein kinase B (AKT/PKB) signaling pathway / glucose transporter-4 (GLUT4) signaling pathway, crucial for insulin-stimulated glucose transport, showed suppression in the T2DM group compared to the Con group in the results of Western Blotting. However, EA, Met, and EA+Met treatments reversed the downregulation of hepatic PI3K, AKT, and GLUT4 protein expression. While the EA+Met group exhibited greater increases in protein expression, the differences were not statistically significant. (Fig. 3C). Additionally, the expression of PI3K/AKT/GLUT4, PPARα/CPT1A signaling pathways was down-regulated, while PGC-1α/PCK2 signaling pathway and SREBP1c expression was upgraded in the EA+Compd C group compared to the EA group, that was consistent with the trend of the results in Figs. 1 and 2. The results indicated that EA alleviated liver injury in T2DM rats through AMPK and downstream glycolipid metabolism and insulin signaling pathways.

EA inhibited hepatic steatosis by activating autophagy mediated by AMPK in T2DM rats

The role of autophagy in T2DM-induced MAFLD emerges as pivotal, serving as a cellular mechanism that mitigates liver steatosis and maintains cellular homeostasis. Transmission electron microscopy revealed pronounced differences between the control and T2DM groups in liver cell composition. In the T2DM group, substantial lipid droplets were evident alongside blurred mitochondrial structure, expanded endoplasmic reticulum, and diminished autophagosomes, whereas EA, Met, and EA+Met groups showed restored cellular morphology with increased autophagosomes and reduced lipid droplets (Fig. 4A). The autophagy activity in liver of T2DM rats was examined by western blotting, qPCR, immunohistochemistry and immunofluorescence. In Fig. 4B-1 [1,2], B-2 [1], B-3 [1,3], a notable downward trend in both protein and mRNA expression of LC3II was observed in the T2DM group, indicating suppressed autophagy activity. Conversely, the EA, Met, and EA+Met groups exhibited a significant upsurge in LC3II expression, suggesting that EA, Met, and EA+Met interventions partially restored autophagy activity impaired by T2DM. In Fig. 4B-3 [1, 3], the EA+Met group was superior to the Met group in increasing liver LC3 expression.

Additionally, to delve deeper into EA's mechanism of action in combating diabetes by ameliorating hepatic lipid accumulation through autophagy, we scrutinized the effects of the AMPK/mTOR pathway in the livers of T2DM rats. The results from Fig. 3A-1, A-2 and Fig. 4B-1 [1, 3], B-2 [2] indicated that HFD+STZ treatment significantly increased p-mTOR/mTOR and mTOR mRNA levels, while decreasing p-AMPK/AMPK and AMPK mRNA levels. Conversely, EA, Met, and EA+Met treatment restored these levels. This suggested that EA might regulate liver autophagy activity through the AMPK/mTOR pathway. Immunohistochemical analysis mirrored the western blotting and qPCR findings for AMPK and mTOR expression in the liver (Fig. 3 and Fig. 4B-3 [2, 4]). This study also showed that Compound C effectively inhibited the promotion of autophagy by EA in liver, including a marked augmented level of mTOR and low expression of LC3II, which could explain the increase of lipid droplet, the decrease of autophagosomes, hepatic morphological damage, and reduced liver fuction.

EA reduces liver fibrosis induced by TGF β1/smad3 pathway in T2DM rats

Similar to the results of Masson staining in Fig. 2C, Transmission electron microscopy revealed significant collagen fibers in the perisinusoidal space of the liver in the T2DM group, a feature notably reduced in the EA, Met, and EA+Met groups (Fig. 5A). The Western blot analysis had showed that the model group exhibited increased α-SMA expression compared to the Con group. However, in the EA, Met, and EA+Met groups, α-SMA expression decreased significantly compared to the model group, indicating three treatment's potential to inhibit hepatic fibrosis, as shown in Fig. 5B-1 [1,2]. This was further supported by the immunofluorescence results (Fig. 5B-2 [1,3]).

The association of the TGFβ1/Smad3 pathway with liver fibrosis has been extensively demonstrated. To investigate whether the protective effect of EA involves inhibition of the TGFβ1/Smad3 pathway, we assessed changes in this pathway using Western blotting, immunohistochemistry, and qPCR methods. Primarily, Western blot and immunohistochemistry analyses revealed significantly elevated expressions of TGFβ1 and Smad3 in the T2DM group compared to the control group (Fig. 5B-1 [1,3,5], 5 B-2 [2, 4]). However, after 6 weeks of EA, Met, and EA+Met treatment, these expressions were notably suppressed. Furthermore, qPCR results mirrored these findings: liver tissue from T2DM rats exhibited increased mRNA expression of TGFβ1, Smad2, and Smad3 (Fig. 5B-3). Yet, treatment with EA, Met, and EA+Met effectively inhibited the mRNA expression of TGFβ1, Smad2, and Smad3. To further identify the involvement of glycolipid metabolism and autophagy mediated by AMPK in

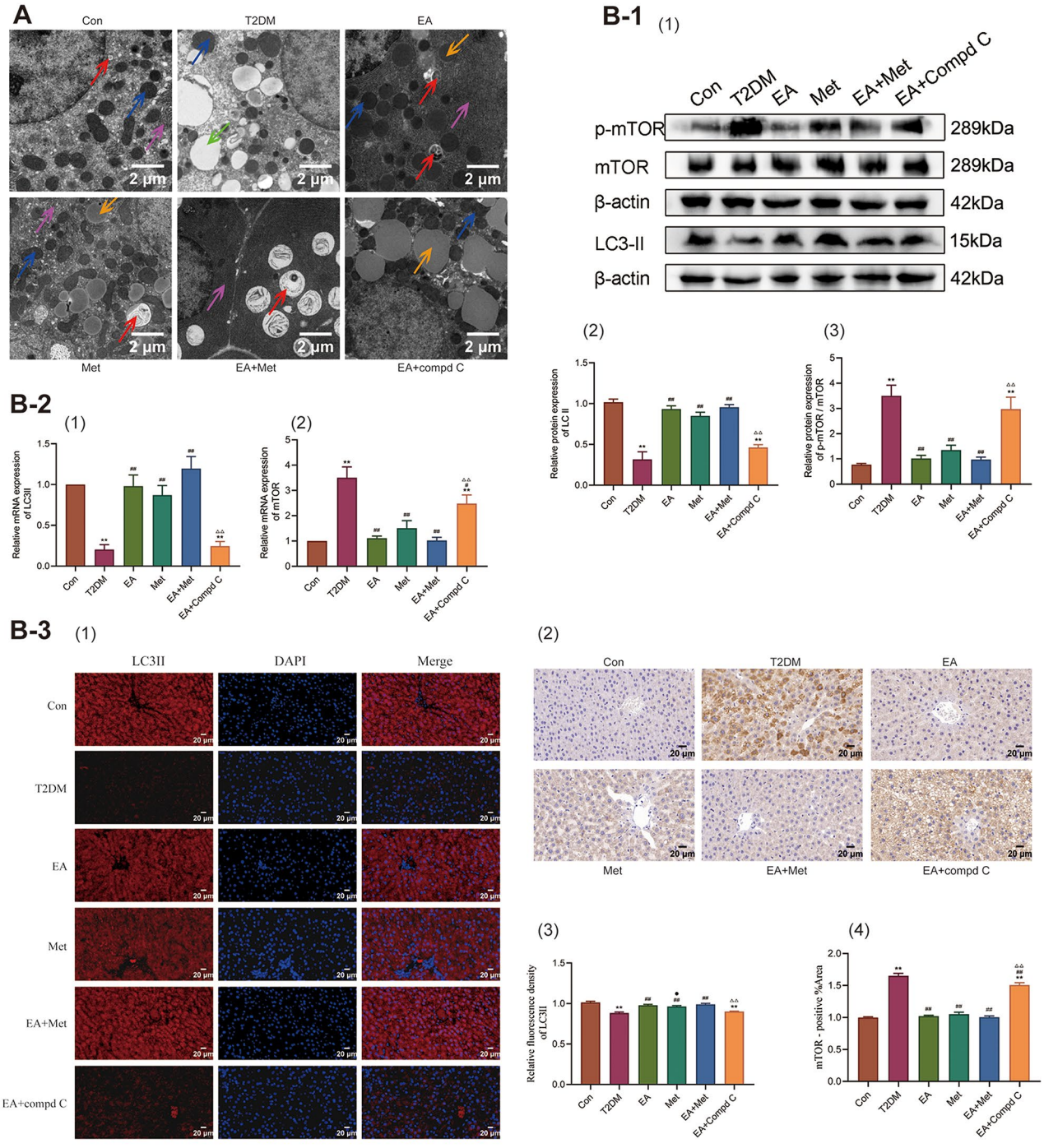

Fig. 4 The effects of EA on hepatic autophagy in T2DM model rats. **A**: Electron microscopy observed autophagy and lipid droplets in liver cells (red arrow: autophagosomes, yellow arrow: lipid droplets, blue arrow: mitochondria, purple arrow: endoplasmic reticulum, green arrow: lipid vacuoles). Images are shown at the original magnification of 15,000×. **B**-1: [1] Protein expression of hepatic autophagy signaling pathway. [2–3] Quantification of protein levels of LC3II, p-mTOR/mTOR ($n=3$ per group). **B**-2: [1–2] mRNA levels of LC3II, mTOR ($n=6$ per group). **B**-3: [1] Representative images of immunofluorescence staining of LC3II expressions in the liver. Images are shown at the original magnification of 400×. [2] Representative images of immunohistochemical staining of mTOR expressions in the liver. Images are shown at the original magnification of 400×. [3–4] Quantitative analyses according to groups ($n=6$ per group). Con: the control group, T2DM: the T2DM group, EA: the electroacupuncture group, Met: the metformin group, EA + Met: combination group of electroacupuncture and metformin, EA + Compd C: combination group of electroacupuncture and compound C. Data are expressed as mean ± standard error of mean. Compared with the Con group, $^{**}P<0.01$; compared with the T2DM group, $^{\#\#}P<0.01$; compared with the EA group, $P<0.01$; compared with the EA + Met group, $P<0.05$

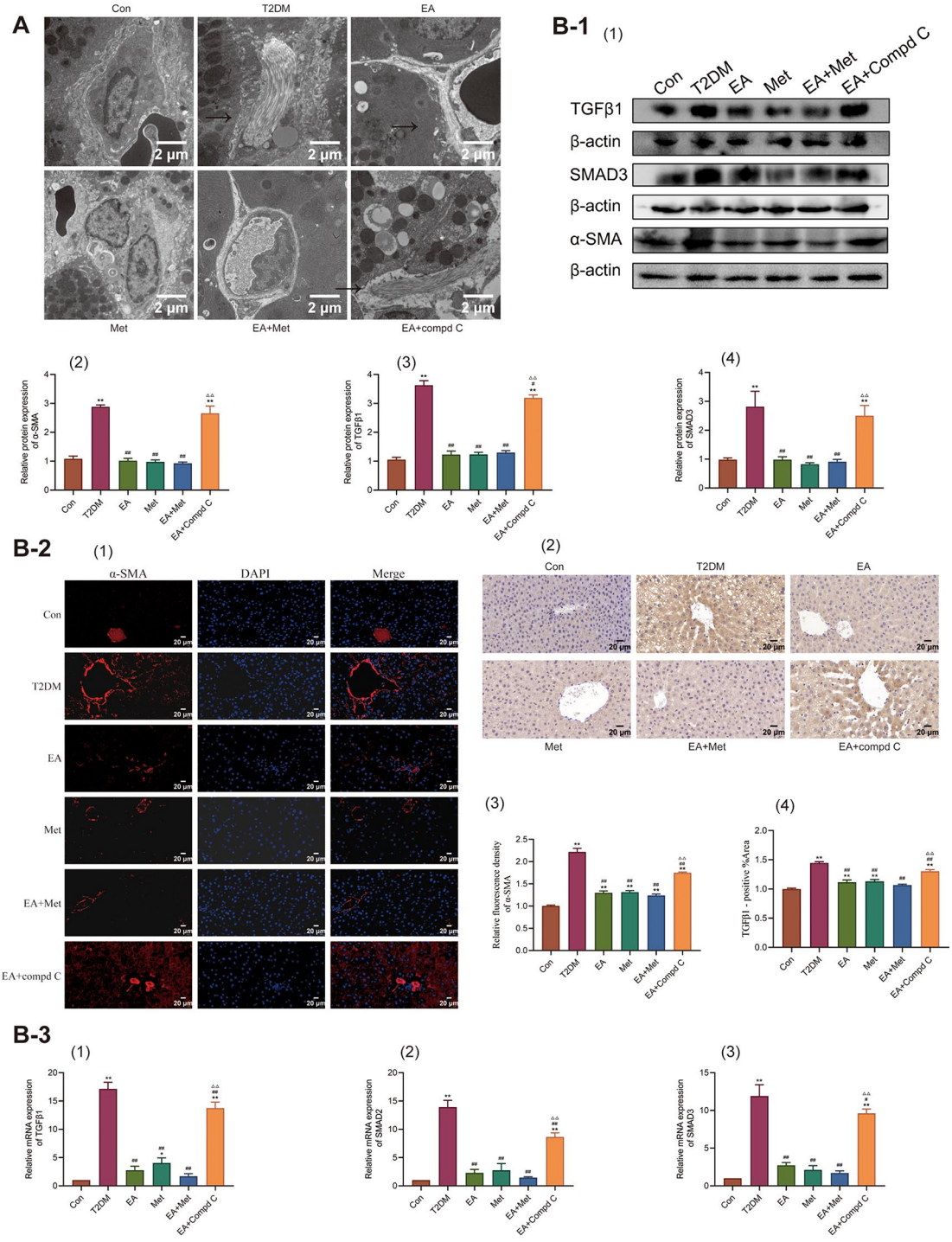

Fig. 5 The effects of EA on liver fibrosis in T2DM model rats. **A**: Electron microscopy observed collagen fibers in liver cells (white arrow: collagen fibers). Images are shown at the original magnification of 15,000×. **B**-1: [1] Protein expression of hepatic fibrosis signaling pathway. [2–4] Quantification of protein levels of α-SMA, TGFβ1, SMAD3 ($n=3$ per group). **B**-2: [1] Representative images of immunofluorescence staining of α-SMA expressions in the liver. Images are shown at the original magnification of 400×. [2] Representative images of immunohistochemical staining of TGFβ1 expressions in the liver. Images are shown at the original magnification of 400×. [3–4] Quantitative analyses according to groups ($n=6$ per group). **B**-3: [1–3] mRNA levels of TGFβ1, SMAD2, SMAD3 ($n=6$ per group). Con: the control group, T2DM: the T2DM group, EA: the electroacupuncture group, Met: the metformin group, EA + Met: combination group of electroacupuncture and metformin, EA + Compd C: combination group of electroacupuncture and compound C. Data are expressed as mean ± standard error of mean. Compared with the Con group, $^{*}P<0.05$, $^{**}P<0.01$; compared with the T2DM group, $^{\#}P<0.05$, $^{\#\#}P<0.01$; compared with the EA group, $P<0.01$

the formation of liver fibrosis, the therapeutic action of EA was further evaluated using intraperitoneal injection of Compound C. The results indicated that the expression of TGFβ1, smad2/3, and α-SMA were significantly increased after EA+Compd C treatment compared with the EA group. Masson staining and transmission electron microscopy showed that the EA+Compd C group exhibited greater degree of collagenous fiber compared with the EA group (Figs. 2C and 5A).

Discussion

Individuals diagnosed with T2DM are susceptible to hepatocyte injury and fibrosis, even when presenting with isolated steatosis in the initial stages. This progression underscores the significance of managing T2DM-induced hepatic steatosis to forestall the development of fibrosis and the onset of MAFLD [50–52]. However, the current clinical landscape is marked by a dearth of FDA-approved drugs specifically tailored for treating MAFLD [32]. Addressing this gap, the present study delved into the protective potential of EA against T2DM-induced hepatic steatosis and ensuing fibrosis.

The AMPK pathway emerges as a pivotal player in bridging the pathophysiological connection between T2DM and MAFLD, orchestrating glycolipid metabolism and insulin resistance [33, 36]. In our study using T2DM rats induced by HFD+STZ treatment, we observed that intervention with EA treatment in T2DM rodent models exhibited hepatoprotective effects by bolstering AMPK activity. Numerous studies emphasized AMPK's pivotal role in T2DM and MAFLD development and progression [53]. AMPK serves as a vital regulator of energy balance in liver, muscle, and adipose tissues [53–55], and modulates energy metabolism by activating catabolic pathways and inhibiting anabolic pathways, including fatty acid oxidation, hepatic lipogenesis, glucose uptake and output, and insulin sensitivity regulation [36]. AMPK phosphorylation inhibits transcription factors that induce gluconeogenesis and lipogenic programs, notably peroxisome proliferator-activated receptor gamma coactivator 1-alpha (PGC-1α), phosphoenolpyruvate carboxykinase 2 (PCK2), and sterol regulatory element-binding protein 1c (SREBP1c), reducing liver glucose and fat accumulation [33, 57]. Additionally, AMPK promotes fatty acid entry into mitochondria and oxidation through the carnitine palmitoyltransferase 1 A (CPT1A) system via peroxisome proliferator-activated receptor α (PPARα) [37], as shown in Fig. 6. Strategies aimed at activating AMPK hold significant promise for both the prevention and treatment of T2DM and MAFLD. In this study, we conducted experiments utilizing T2DM rat models subjected to EA treatment, assessing the relationship between

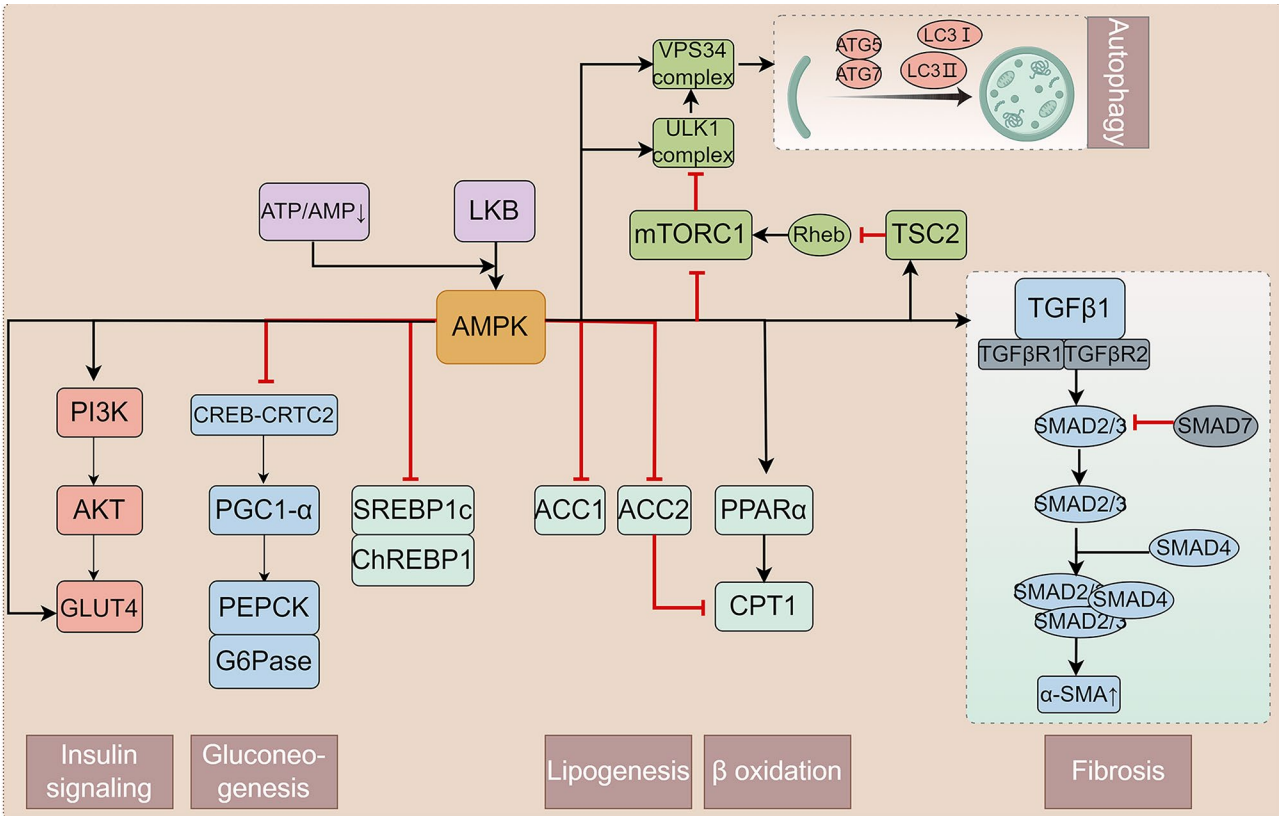

Fig. 6 The relationship between AMPK and metabolic signaling pathways

MAFLD induced by T2DM and expression of molecular markers associated with AMPK. Throughout our rigorous investigation, manifestation of evident IR and dysregulation in glycolipid metabolism within the T2DM rat models. Following a 6-week intervention period, all three treatment modalities not only induced a substantial decrease in FBG levels from the fourth to sixth week but also precipitated a remarkable reduction in TC, TG, LDL, and HOMA-IR levels, coupled with a significant elevation in HDL and HOMA-ISI levels. To assess the impact of T2DM on the liver, we examined liver function and pathological changes. Our observations revealed elevated levels of ALT and AST, alongside reduced ALB levels in T2DM rats compared to the control group. Notably, the livers exhibited lipid vacuoles, ballooning, significant fat accumulation and collagen fibers, indicating liver metabolic dysfunction, hepatocyte steatosis and fibrosis. Furthermore, our results indicated that the three treatments effectively alleviated liver injury induced by IR. This was evidenced by decreased AST and ALT levels, increased ALB levels in serum, and improvements in hepatic morphology, along with reduced areas of positive Oil Red O and Masson staining. These salutary effects were consonant with the activation of AMPK, which in turn promoted the expression of PPARα/CPT1A and PI3K/AKT pathways, inhibited the expression of SREBP1c and PGC-1α/PCK2 pathway, led to diminished adipogenesis and gluconeogenesis, augmented fatty acid oxidation, and heightened insulin sensitivity, thereby substantiating the therapeutic potential of AMPK activation in ameliorating the metabolic derangements associated with T2DM and MAFLD. The regulatory impact of EA, when combined with Met intervention, on the expression of hepatic AMPK surpassed that of both EA and Met administration. This superiority underscored the potential advantage of integrating EA with Met therapy in clinical practice.

Moreover, electron microscope analysis revealed a notable presence of autophagosomes in liver tissue across the three treatment groups. Autophagy, an essential system for maintaining cellular homeostasis, mitigates liver injury, oxidative stress, and inflammation by breaking down and recycling misfolded proteins and damaged organelles resulting from lipid peroxidation [24, 28]. Lipophagy, a subtype of autophagy, targets intracellular lipid droplets (LDs) for degradation, aiming to regulate liver fat stores [25, 26, 58]. Research indicated that compromised autophagic flux contributed to lipid droplet accumulation in hepatocytes, exacerbating hepatic steatosis and damage in T2DM rats. LC3-II, a protein crucial for autophagosome formation and maturation, serves as a reliable marker for assessing autophagic activity [59, 60]. In the present study, both the protein and mRNA expression levels of LC3-II were significantly reduced in the T2DM group, suggesting suppressed autophagic activation. This finding correlated with the observed increase in hepatic lipid deposition and morphological alterations. Conversely, LC3B-II levels were markedly elevated, accompanied by a reduction in LDs following the three treatments compared to the T2DM group. This suggested that enhanced autophagy facilitated lipid clearance in the liver. Central to the regulation of autophagy in MAFLD is the AMPK / mammalian target of rapamycin (mTOR) pathway, which has been extensively documented [61]. mTORC1, a complex of mTOR [62], phosphorylates ULK1 at Ser757, impeding its interaction with AMPK, thus halting autophagy. AMPK, as the upstream regulator of mTOR, negatively modulates mTOR activation either directly by phosphorylating mTORC1 or by phosphorylating various components of mTORC1. Moreover, AMPK fosters autophagy by directly activating ULK1 through phosphorylation at Ser555 and Ser777, facilitating the release of ULK1 from mTORC1. Consequently, the activated ULK1 kinase complex recruits other autophagy proteins, instigating autophagy induction [61–65]. However, in conditions such as steatosis and hypernutrition, autophagy initiation is hindered due to alterations in AMPK and mTOR signaling. The current study revealed a significant decrease in the p-AMPK/AMPK ratio and AMPK mRNA alongside a remarkable increase in the p-mTOR/mTOR ratio and mTOR mRNA. This was coupled with the inhibition of autophagy, as evidenced by the notable decrease in LC3-II levels in the T2DM group. However, autophagy was restored in the groups treated with EA, Met, and EA+Met, achieved through elevated AMPK expression and reduced mTOR expression levels, consequently leading to increased LC3-II levels. Moreover, our results showed that EA-induced autophagy and improvement of hepatic lipid droplet accumulation and glycolipid metabolism was partly disrupted by Compound C, an inhibitor of AMPK, in the EA+Compd C group. Taken together, these results suggest that the beneficial effects of EA may stem from enhanced autophagy via the AMPK/mTOR pathway.

Chronic liver injury caused by T2DM and metabolic disorders gradually progresses to fibrosis, which is characterized by excess deposition of collagen between hepatocytes and hepatic sinusoids to repair the liver damage [67]. In the liver, hepatic stellate cells (HSCs) emerge as the primary source of collagen synthesis, playing a critical role in the dynamic equilibrium of ECM turnover and regulation. In response to liver injury, HSCs undergo a phenotypic transformation into activated myofibroblast-like cells (MFCs), which are proficient in ECM production, notably collagen types I and III, and formate α-smooth muscle actin (α-SMA) stress fibers [68, 69]. Central to the fibrotic cascade is the multifaceted cytokine transforming growth factor-beta (TGF-β), which

synthesized by both liver parenchymal cells and activated HSCs, exerting its effects through a Smad3-dependent signaling pathway [70, 71]. Upon binding to the TGF-β II receptor on the cell membrane of HSCs, TGF-β1 initiates a signaling cascade culminating in the activation of intracellular mediators, notably Smad proteins [72]. Subsequently, the Smad complex, comprising Smad2, Smad3, and Smad4, translocates into the nucleus, where it exerts transcriptional control by directly binding to the collagen promoter region, thereby fostering ECM production and deposition, thereby perpetuating the fibrotic response in the liver [73, 74]. Our results showed that the expressions of α-SMA, a fibroblast marker, were abundantly increased in the T2DM group. The pathological characteristics of T2DM in massson staining and electron-microscope exhibited an increase in hepatic fibrosis, indicating activation of HSCs. We also found that HFD + STZ treatment distinctly increased the expressions of TGFβ1, smad2, and smad3. These data prompted that T2DM-induced aberrant glycolipid metabolism possess a critical role in liver injury and fibrosis in T2DM rats. It is worth mentioning that the three treatments could attenuated this effect and significantly ameliorate hepatic fibrosis and decrease the expression of TGFβ1, smad2, and smad3 in T2DM rats, suggesting that the antifibrotic activity of three treatments may be associated, at least partially, with TGFβ1/smad2/3 signaling pathway activity attenuation.

Metformin, a cornerstone medication in T2DM management, operates through the activation of the AMPK pathway, thereby enhancing liver function and insulin sensitivity [75, 76]. Experimental studies have reported that metformin has beneficial effects on improving hepatic steatosis and fibrosis in T2DM. However, reliable clinical data on metformin treatment for hepatic fibrosis in MAFLD patients are lacking, so international societies do not recommend metformin as a treatment for MAFLD. This study investigated the effects of metformin on liver injury and AMPK-related pathway expression in T2DM rats and endeavored to elucidate whether the combined administration of EA and metformin yields synergistic effects. We found that there were no significant differences among the three treatment groups in improving glucose and lipid metabolism and insulin sensitivity. However, EA + Met group had advantages in improving liver morphology and liver function (ALT), particularly in improving the morphology and quantity of the endoplasmic reticulum. This may be due to the synergistic effect of EA + Met in increasing the expression of hepatic AMPK and LC3-II.

However, there arised a question: was the upregulation of autophagy and glycolipid metabolism by EA linked to the downregulation of TGFβ1/SMAD3 signaling, or was it an independent molecular event requiring further investigation? As previously mentioned, AMPK-mediated glycolipid metabolism and autophagy contributed to restoring liver structure and function, thereby preventing liver fibrosis by mitigating factors causing liver damage. In our present study, as anticipated, the introduction of Compound C, an AMPK inhibitor, suppressed AMPK activation and partially reversed the beneficial effects of EA on the TGFβ1/SMAD3 signaling pathway and liver fibrosis. This finding confirmed a direct relationship between AMPK activation and the anti-fibrotic effects of EA treatment. Considering the aforementioned studies, the AMPK signaling pathway mediated EA's beneficial effects in delaying the progression of MAFLD in T2DM rats.

In conclusion, to the best of our knowledge, the results of the present study showed that EA played a critical role in ameliorating in MAFLD in T2DM rats. Specifically, EA intervention improved FBG, serum lipids, insulin sensitivity and hepatic function, and inhabited liver steatosis and fibrosis of T2DM rats. Furthermore, we demonstrated insights that EA treatment was likely through the mechanisms of the up-regulating of hepatic AMPK signaling pathway, which mediated glycolipid metabolism and autophagy, inhibited TGFβ1/SMAD3 pathway-induced fibrosis. Moreover, the above effects of EA were consistent with metformin. The combination of EA and metformin had significant advantages in increasing hepatic AMPK expression, improving liver morphology, lipid droplet infiltration, fibrosis, and reducing serum ALT levels. Taken together, our findings indicated that EA might be taken as an effective therapeutic strategy and improving the efficacy of metformin in MAFLD. Therefore, the combined approach of EA and Met in clinical practice offers a personalized and holistic treatment strategy that considers the individual's constitutional differences and the dynamic nature of metabolic disorders. Through synergistic interactions, acupuncture may enhance the efficacy of pharmacotherapy while minimizing adverse effects and promoting overall well-being. Future research endeavors should focus on elucidating the underlying mechanisms responsible for the superior regulatory effect of EA combined with Met on liver AMPK expression. Additionally, multiple animal studies and larger clinical trials are warranted to validate the therapeutic efficacy and safety of this integrated approach in diverse patient populations with metabolic disorders.

Supplementary Information

The online version contains supplementary material available at https://doi.org/10.1186/s13098-024-01432-7.

Supplementary Material 1

Acknowledgements
The authors thank the School of Acupuncture - Moxibustion, and Tuina, Beijing University of Chinese Medicine for supplied experimental equipment and research environment.

Author contributions
HD: Conceptualization, Writing—original draft, Project administration. SS: Data curation, Methodology. RL: Supervision, Funding acquistion. SH: Writing – review & editing. SZ: Visualization. SL: Software. XL: Formal analysis. WG: Validation.

Funding
This study was supported by the following grants: (1) National Natural Science Foundation of China (Grant Nos. 81973935); (2) Beijing Municipal Natural Science Foundation (Grant Nos. 7232276).

Data availability
The datasets used and/or analyzed during the current study are available from the corresponding author upon reasonable request.

Declarations

Ethical approval
The protocol received approval from the Laboratory Animal Welfare and Ethics Committee of Beijing University of Chinese Medicine (BUCM-4-2021051301-2026).

Competing interests
The authors declare no competing interests.

Author details
[1]School of Acupuncture - Moxibustion, and Tuina, Beijing University of Chinese Medicine, Beijing 100029, China
[2]Department of Acupuncture and Moxibustion, Chaoyang District Traditional Chinese Medicine Hospital, Beijing 100026, China
[3]Department of Acupuncture and Moxibustion, China- Japan Friendship Hospital, Beijing 100029, China
[4]Department of Gastroenterology, Henan Province Hospital of Traditional Chinese Medicine, Henan University of Chinese Medicine, Henan 450002, China

Received: 25 May 2024 / Accepted: 24 July 2024
Published online: 11 September 2024

References

1. Muthiah MD, Cheng Han N, Sanyal AJ. A clinical overview of non-alcoholic fatty liver disease: a guide to diagnosis, the clinical features, and complications-what the non-specialist needs to know. Diabetes Obes Metab. 2022;24(Suppl 2):3–14.
2. Ahmad E, Lim S, Lamptey R, Webb DR, Davies MJ. Type 2 diabetes. Lancet (London England). 2022;400(10365):1803–20.
3. Xie J, Huang H, Liu Z, Li Y, Yu C, Xu L, et al. The associations between modifiable risk factors and nonalcoholic fatty liver disease: a comprehensive mendelian randomization study. Hepatology (Baltimore MD). 2023;77(3):949–64.
4. Butt AS, Hamid S, Haider Z, Sharif F, Salih M, Awan S, et al. Nonalcoholic fatty liver diseases among recently diagnosed patients with diabetes Mellitus and Risk factors. Euroasian J hepato-gastroenterology. 2019;9(1):9–13.
5. Santos RD, Valenti L, Romeo S. Does nonalcoholic fatty liver disease cause cardiovascular disease? Current knowledge and gaps. Atherosclerosis. 2019;282:110–20.
6. Brouwers MCGJ, Simons N, Stehouwer CDA, Isaacs A. Non-alcoholic fatty liver disease and cardiovascular disease: assessing the evidence for causality. Diabetologia. 2020;63(2):253–60.
7. Biondi-Zoccai GGL, Abbate A, Liuzzo G, Biasucci LM. Atherothrombosis, inflammation, and diabetes. J Am Coll Cardiol. 2003;41(7):1071–7.
8. Cusi K. Treatment of patients with type 2 diabetes and non-alcoholic fatty liver disease: current approaches and future directions. Diabetologia. 2016;59(6):1112–20.
9. Targher G, Bertolini L, Poli F, Rodella S, Scala L, Tessari R, et al. Nonalcoholic fatty liver Disease and Risk of Future Cardiovascular events among type 2 Diabetic patients. Diabetes. 2005;54(12):3541–6.
10. Perry RJ, Samuel VT, Petersen KF, Shulman GI. The role of hepatic lipids in hepatic insulin resistance and type 2 diabetes. Nature. 2014;510(7503):84–91.
11. Jung I, Koo DJ, Lee WY. Insulin Resistance, non-alcoholic fatty liver disease and type 2 diabetes Mellitus: clinical and experimental perspective. Diabetes & metabolism journal; 2024.
12. Donnelly KL, Smith CI, Schwarzenberg SJ, Jessurun J, Boldt MD, Parks EJ. Sources of fatty acids stored in liver and secreted via lipoproteins in patients with nonalcoholic fatty liver disease. J Clin Investig. 2005;115(5):1343–51.
13. Roden M. Mechanisms of Disease: hepatic steatosis in type 2 diabetes–pathogenesis and clinical relevance. Nat Clin Pract Endocrinol Metab. 2006;2(6):335–48.
14. Sekizkardes H, Chung ST, Chacko S, Haymond MW, Startzell M, Walter M, et al. Free fatty acid processing diverges in human pathologic insulin resistance conditions. J Clin Investig. 2020;130(7):3592–602.
15. Birkenfeld AL, Shulman GI. Nonalcoholic fatty liver disease, hepatic insulin resistance, and type 2 diabetes. Hepatology (Baltimore MD). 2014;59(2):713–23.
16. Lam TK, Carpentier A, Lewis GF, van de Werve G, Fantus IG, Giacca A. Mechanisms of the free fatty acid-induced increase in hepatic glucose production. Am J Physiol Endocrinol Metabolism. 2003;284(5):E863–73.
17. Koliaki C, Szendroedi J, Kaul K, Jelenik T, Nowotny P, Jankowiak F, et al. Adaptation of hepatic mitochondrial function in humans with non-alcoholic fatty liver is lost in steatohepatitis. Cell Metabol. 2015;21(5):739–46.
18. Morgan MJ, Liu ZG. Crosstalk of reactive oxygen species and NF-κB signaling. Cell Res. 2011;21(1):103–15.
19. Cohen JC, Horton JD, Hobbs HH. Human fatty liver disease: old questions and new insights. Sci (New York NY). 2011;332(6037):1519–23.
20. Chalasani N, Younossi Z, Lavine JE, Charlton M, Cusi K, Rinella M, et al. The diagnosis and management of nonalcoholic fatty liver disease: practice guidance from the American Association for the study of Liver diseases. Hepatology (Baltimore MD). 2018;67(1):328–57.
21. Bedossa P, Poitou C, Veyrie N, Bouillot JL, Basdevant A, Paradis V, et al. Histopathological algorithm and scoring system for evaluation of liver lesions in morbidly obese patients. Hepatology (Baltimore MD). 2012;56(5):1751–9.
22. Ellis EL, Mann DA. Clinical evidence for the regression of liver fibrosis. J Hepatol. 2012;56(5):1171–80.
23. Wong RJ, Aguilar M, Cheung R, Perumpail RB, Harrison SA, Younossi ZM, et al. Nonalcoholic steatohepatitis is the second leading etiology of liver disease among adults awaiting liver transplantation in the United States. Gastroenterology. 2015;148(3):547–55.
24. He C, Zheng X, Lin X, Chen X, Shen C. Yunvjian-Medicated Serum Protects INS-1 Cells against Glucolipotoxicity-Induced Apoptosis through Autophagic Flux Modulation. Evidence-based complementary and alternative medicine: eCAM. 2020;2020:8878259.
25. Hosaka Y, Araya J, Fujita Y, Kuwano K. Role of chaperone-mediated autophagy in the pathophysiology including pulmonary disorders. Inflamm Regeneration. 2021;41(1):29.
26. Kawabata T, Yoshimori T. Autophagosome biogenesis and human health. Cell Discovery. 2020;6(1):33.
27. González-Rodríguez A, Mayoral R, Agra N, Valdecantos MP, Pardo V, Miquilena-Colina ME, et al. Impaired autophagic flux is associated with increased endoplasmic reticulum stress during the development of NAFLD. Cell Death Dis. 2014;5(4):e1179.
28. Czaja MJ. Function of Autophagy in nonalcoholic fatty liver disease. Dig Dis Sci. 2016;61(5):1304–13.
29. Zai W, Chen W, Luan J, Fan J, Zhang X, Wu Z, et al. Dihydroquercetin ameliorated acetaminophen-induced hepatic cytotoxicity via activating JAK2/STAT3 pathway and autophagy. Appl Microbiol Biotechnol. 2018;102(3):1443–53.
30. Wang K. Autophagy and apoptosis in liver injury. Cell Cycle (Georgetown Tex). 2015;14(11):1631–42.
31. Ni HM, Woolbright BL, Williams J, Copple B, Cui W, Luyendyk JP, et al. Nrf2 promotes the development of fibrosis and tumorigenesis in mice with defective hepatic autophagy. J Hepatol. 2014;61(3):617–25.
32. EASL-EASD-EASO. Clinical practice guidelines for the management of non-alcoholic fatty liver disease. Diabetologia. 2016;59(6):1121–40.
33. Hardie DG, Schaffer BE, Brunet A. AMPK: an energy-sensing pathway with multiple inputs and outputs. Trends Cell Biol. 2016;26(3):190–201.
34. Jiang SJ, Dong H, Li JB, Xu LJ, Zou X, Wang KF, et al. Berberine inhibits hepatic gluconeogenesis via the LKB1-AMPK-TORC2 signaling

pathway in streptozotocin-induced diabetic rats. World J Gastroenterol. 2015;21(25):7777–85.
35. Lee JM, Seo WY, Song KH, Chanda D, Kim YD, Kim DK, et al. AMPK-dependent repression of hepatic gluconeogenesis via disruption of CREB.CRTC2 complex by orphan nuclear receptor small heterodimer partner. J Biol Chem. 2010;285(42):32182–91.
36. Day EA, Ford RJ, Steinberg GR. AMPK as a therapeutic target for treating metabolic diseases. Trends Endocrinol Metab. 2017;28(8):545–60.
37. Sayeed M, Gautam S, Verma DP, Afshan T, Kumari T, Srivastava AK, et al. A collagen domain-derived short adiponectin peptide activates APPL1 and AMPK signaling pathways and improves glucose and fatty acid metabolisms. J Biol Chem. 2018;293(35):13509–23.
38. Behrends C, Sowa ME, Gygi SP, Harper JW. Network organization of the human autophagy system. Nature. 2010;466(7302):68–76.
39. Alers S, Löffler AS, Wesselborg S, Stork B. Role of AMPK-mTOR-Ulk1/2 in the regulation of autophagy: cross talk, shortcuts, and feedbacks. Mol Cell Biol. 2012;32(1):2–11.
40. Jakobsen SN, Hardie DG, Morrice N, Tornqvist HE. 5'-AMP-activated protein kinase phosphorylates IRS-1 on Ser-789 in mouse C2C12 myotubes in response to 5-aminoimidazole-4-carboxamide riboside. J Biol Chem. 2001;276(50):46912–6.
41. Qu W, Ma T, Cai J, Zhang X, Zhang P, She Z, et al. Liver fibrosis and MAFLD: from Molecular aspects to Novel pharmacological strategies. Front Med. 2021;8:761538.
42. Liu XX, Zhang LZ, Zhang HH, Lai LF, Wang YQ, Sun J, et al. Low-frequency electroacupuncture improves disordered hepatic energy metabolism in insulin-resistant Zucker diabetic fatty rats via the AMPK/mTORC1/p70S6K signaling pathway. Acupunct Medicine: J Br Med Acupunct Soc. 2022;40(4):360–8.
43. Tian HH, Cao BY, Li R, Ma YJ, Hu XG, Jia N, et al. Effects of electroacupuncture stimulation at different spinal segmental levels in a rat model of diabetes mellitus. Acupunct Medicine: J Br Med Acupunct Soc. 2018;36(1):29–35.
44. Kang Y, Li M, Yan W, Li X, Kang J, Zhang Y. Electroacupuncture alters the expression of genes associated with lipid metabolism and immune reaction in liver of hypercholesterolemia mice. Biotechnol Lett. 2007;29(12):1817–24.
45. Martinez B, Peplow PV. Treatment of insulin resistance by acupuncture: a review of human and animal studies. Acupunct Medicine: J Br Med Acupunct Soc. 2016;34(4):310–9.
46. Ma B, Li P, An H, Song Z. Electroacupuncture attenuates liver inflammation in nonalcoholic fatty liver disease rats. Inflammation. 2020;43(6):2372–8.
47. Jiang H, Shang Z, You L, Zhang J, Jiao J, Qian Y, et al. Electroacupuncture pretreatment at Zusanli (ST36) ameliorates hepatic Ischemia/Reperfusion Injury in mice by reducing oxidative stress via activating Vagus nerve-dependent Nrf2 pathway. J Inflamm Res. 2023;16:1595–610.
48. WU K K HUANY. Streptozotocin-Induced Diabetic models in mice and rats [J]. Curr Protocols Pharmacol, 2008, 40(1): 5.47.41–45.47.14.
49. WANG Y, RIJAL B, XU M, et al. Renal denervation improves vascular endothelial dysfunction by inducing autophagy via AMPK/mTOR signaling activation in a rat model of type 2 diabetes mellitus with insulin resistance [J]. Acta diabetologica, 2020, 57(10): 1227-1243.50.
50. Singh S, Allen AM, Wang Z, Prokop LJ, Murad MH, Loomba R. Fibrosis progression in nonalcoholic fatty liver vs nonalcoholic steatohepatitis: a systematic review and meta-analysis of paired-biopsy studies. Clinical gastroenterology and hepatology: the official clinical practice. J Am Gastroenterol Assoc. 2015;13(4):643–54.e1-9.
51. Taylor RS, Taylor RJ, Bayliss S, Hagström H, Nasr P, Schattenberg JM, et al. Association between Fibrosis Stage and outcomes of patients with nonalcoholic fatty liver disease: a systematic review and Meta-analysis. Gastroenterology. 2020;158(6):1611–e2512.
52. Mantovani A, Byrne CD, Bonora E, Targher G. Nonalcoholic fatty liver disease and risk of Incident Type 2 diabetes: a Meta-analysis. Diabetes Care. 2018;41(2):372–82.
53. Fullerton MD, Galic S, Marcinko K, Sikkema S, Pulinilkunnil T, Chen Z-P, et al. Single phosphorylation sites in Acc1 and Acc2 regulate lipid homeostasis and the insulin-sensitizing effects of metformin. Nat Med. 2013;19(12):1649–54.
54. Xiao B, Sanders MJ, Carmena D, Bright NJ, Haire LF, Underwood E, et al. Structural basis of AMPK regulation by small molecule activators. Nat Commun. 2013;4:3017.
55. Liang J, Xu ZX, Ding Z, Lu Y, Yu Q, Werle KD, et al. Myristoylation confers noncanonical AMPK functions in autophagy selectivity and mitochondrial surveillance. Nat Commun. 2015;6:7926.
56. Garcia D, Shaw RJ. AMPK: mechanisms of Cellular Energy Sensing and Restoration of metabolic balance. Mol Cell. 2017;66(6):789–800.
57. Li Y, Xu S, Mihaylova MM, Zheng B, Hou X, Jiang B, et al. AMPK phosphorylates and inhibits SREBP activity to attenuate hepatic steatosis and atherosclerosis in diet-induced insulin-resistant mice. Cell Metabol. 2011;13(4):376–88.
58. Grefhorst A, van de Peppel IP, Larsen LE, Jonker JW, Holleboom AG. The role of Lipophagy in the development and treatment of non-alcoholic fatty liver disease. Front Endocrinol. 2020;11:601627.
59. Xun Q, Kuang J, Yang Q, Wang W, Zhu G. GLCCI1 reduces collagen deposition and airway hyper-responsiveness in a mouse asthma model through binding with WD repeat domain 45B. J Cell Mol Med. 2021;25(14):6573–83.
60. Zhang E, Yin S, Song X, Fan L, Hu H. Glycycoumarin inhibits hepatocyte lipoapoptosis through activation of autophagy and inhibition of ER stress/GSK-3-mediated mitochondrial pathway. Sci Rep. 2016;6:38138.
61. Cao W, Li J, Yang K, Cao D. An overview of autophagy: mechanism, regulation and research progress. Bull Cancer. 2021;108(3):304–22.
62. Inoki K, Kim J, Guan KL. AMPK and mTOR in cellular energy homeostasis and drug targets. Annu Rev Pharmacol Toxicol. 2012;52:381–400.
63. Juszczak F, Caron N, Mathew AV, Declèves AE. Critical role for AMPK in Metabolic Disease-Induced chronic kidney disease. Int J Mol Sci. 2020;21(21):7994.
64. Kim J, Kundu M, Viollet B, Guan KL. AMPK and mTOR regulate autophagy through direct phosphorylation of Ulk1. Nat Cell Biol. 2011;13(2):132–41.
65. Zhou C, Ma K, Gao R, Mu C, Chen L, Liu Q, et al. Regulation of mATG9 trafficking by src- and ULK1-mediated phosphorylation in basal and starvation-induced autophagy. Cell Res. 2017;27(2):184–201.
66. Mansueto G, Armani A, Viscomi C, D'Orsi L, De Cegli R, Polishchuk EV, et al. Transcription factor EB controls metabolic flexibility during Exercise. Cell Metabol. 2017;25(1):182–96.
67. Roehlen N, Crouchet E, Baumert TF. Liver fibrosis: mechanistic concepts and therapeutic perspectives. Cells. 2020;9(4):875.
68. Josan S, Billingsley K, Orduna J, Park JM, Luong R, Yu L, et al. Assessing inflammatory liver injury in an acute CCl4 model using dynamic 3D metabolic imaging of hyperpolarized [1-(13)C]pyruvate. NMR Biomed. 2015;28(12):1671–7.
69. Khomich O, Ivanov AV, Bartosch B. Metabolic hallmarks of hepatic stellate cells in liver fibrosis. Cells. 2019;9(1):24.
70. Kisseleva T, Brenner D. Molecular and cellular mechanisms of liver fibrosis and its regression. Nat Reviews Gastroenterol Hepatol. 2021;18(3):151–66.
71. Zisser A, Ipsen DH, Tveden-Nyborg P. Hepatic stellate cell activation and inactivation in NASH-Fibrosis-roles as putative treatment targets? Biomedicines. 2021;9(4):365.
72. Diao J, Chen X, Jiang L, Mou P, Wei R. Transforming growth factor-β1 suppress pentraxin-3 in human orbital fibroblasts. Endocrine. 2020;70(1):78–84.
73. Zhang YE. Non-smad Signaling pathways of the TGF-β family. Cold Spring Harb Perspect Biol. 2017;9(2):a022129.
74. Liu T, Xu L, Wang C, Chen K, Xia Y, Li J, et al. Alleviation of hepatic fibrosis and autophagy via inhibition of transforming growth factor-β1/Smads pathway through shikonin. J Gastroenterol Hepatol. 2019;34(1):263–76.
75. Ruan G, Wu F, Shi D, Sun H, Wang F, Xu C. Metformin: update on mechanisms of action on liver diseases. Front Nutr. 2023;10:1327814.
76. Zhang CS, Li M, Ma T, Zong Y, Cui J, Feng JW, et al. Metformin activates AMPK through the Lysosomal Pathway. Cell Metabol. 2016;24(4):521–2. Supplementary Material.

Publisher's Note